IOP Conf. Series: Materials Science and Engineering **580** (2019) 012017 doi:10.1088/1757-899X/580/1/012017

Using synchrotron radiation to improve understanding of deformation of polycrystalline metals by measuring, modelling and publishing 4D information

D Greeley[1], M Yaghoobi[1], D Pagan[2], V Sundararaghavan[1] and J Allison[1]

[1]University of Michigan, Ann Arbor, MI
[2]Cornell High Energy Syncrotron Source, Cornell University, Ithaca, NY

E-mail: johnea@umich.edu

Abstract. The evolution of deformation in a Mg-Nd alloy has been investigated using 3D HEDM and crystal plasticity simulation using the *PRISMS-Plasticity* CPFE Code. Using a simplified representative volume element (RVE), the average stress-strain response is well predicted by the *PRISMS-Plasticity* simulation. The distribution of the resolved shear stresses corresponding to the basal mode for all grains is obtained using both HEDM and the CPFE. simulation. The results show that the CPFE predicted substantially narrower distributions, thus indicating the need for improved digital representation of the RVE. The results of these HEDM experiments and *PRISMS-Plasticity* simulations have been stored in the Materials Commons in a straight-forward manner and are being made available as a published dataset. Both *PRISMS-Plasticity* and the Materials Commons are open-source and available for use by the global materials community.

1. Introduction

The Center for PRedictive Integrated Structural Materials Science (PRISMS) is a major software innovation center that is a component of the US Materials Genome Initiative. The PRISMS Center is developing a framework comprised of advanced open-source multi-scale software integrated with experiments and a data repository, the Materials Commons, to accelerate the predictive science for structural metals [1]. The open-source software includes real space density functional software, a statistical mechanics code, a phase field code and crystal plasticity software. In this paper we present an overview of one project within the Center, the use of high energy x-ray diffraction (HEXD) to map the evolution of local strains with time (the fourth dimension) measured in 3D coupled with simulation of this strain evolution using the *PRISMS-Plasticity* open source full field crystal plasticity finite element code. The results of both are stored and being published as a public dataset using the Materials Commons. This research project is investigating grain size effects on monotonic and cyclic deformation in a Mg-Nd alloy. This paper describes initial results of simulations and experimental results on tensile behaviour of this alloy.

2. Experimental

2.1 Materials

The material used in this experiment was extruded Mg-2.4 weight percent Nd (Mg-2.4Nd), provided by CanmetMATERIALS. Samples were solution heat treated at 525°C for 30 minutes, with an average grain size of 145μm. Mechanical test specimens were wire electrical discharge machined with the loading direction aligned parallel to the bar extrusion direction. Test specimens were machined with a gage cross section of 1mm x 1mm, and a gage length of 1.52mm.

2.2 Experimental Setup

High energy X-ray diffraction microscopy (HEDM) measurements were performed at Sector ID1-A3 beamline at the Cornell High Energy Synchrotron Source (CHESS). A solution heat treated (SHT) Mg-2.4Nd specimen was imaged through a single displacement-controlled, uniaxial tensile loading to track grain scale deformation evolution. Mechanical loading was performed on the Rotational and Axial Motion System, 2nd Build (RAMS2) load frame [2] with the experimental test setup shown in Figure 1. The validity of this experimental framework to measure the average grain strain has been demonstrated by Pagan et al. [3-5].

Samples were displaced uniaxially in the RAMS2 load frame with macroscopic stress measured through a load cell and macroscopic strain measured through surface digital image correlation (DIC) measurements. Far-field high energy X-ray diffraction microscopy (ff-HEDM) measurements were obtained at load steps corresponding to 0.2 and 0.5% macroscopic strain in tension. Six 150μm-height layers were imaged and stacked to illuminate a 1mm x 1mm x 0.9mm volume of the gage section. The samples were box beam scanned with a beam energy of 41.991 keV, and the illuminated volume location was tracked with a surface fiducial wire marker. At each HEDM measurement load step, the specimens were unloaded by 15% to avoid stress relaxation during diffraction imaging. Far-field diffraction patterns were captured at 0.25° increments over a 360° specimen rotation on two Dexela 2923 NDT panel detectors located 878mm from the test specimen.

High energy x-ray diffraction data was processed and reconstructed using the HEXRD software package [6]. Grain center of mass, average crystallographic orientation, and elastic strain tensor were tracked at each load step for 376 grains in the SHT condition through spot analysis of far-field diffraction peak position.

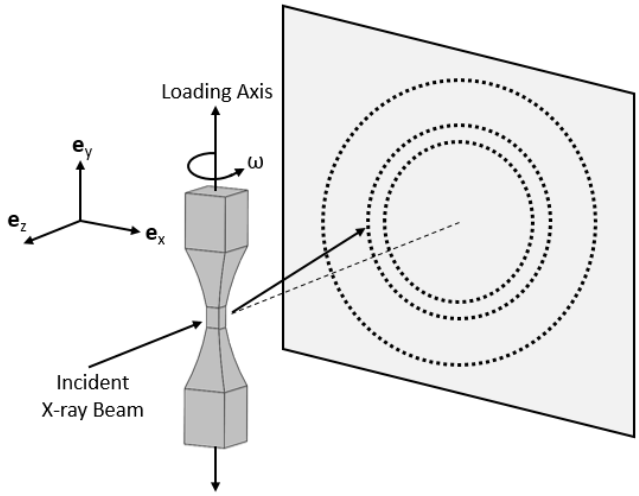

Figure 1. Test geometry in the far-field diffraction condition. Laboratory coordinates are listed, with the beam direction along z and tensile axis along y.

3. *PRISMS-Plasticity* Crystal plasticity model and model set-up

The open-source parallel 3-D crystal plasticity finite element (CPFE) software package *PRISMS-Plasticity* [7] was used to capture the sample response and evolution of slip system strengths. This code is available on Github at prisms-center/plasticity. The constitutive model of each grain is modelled using the rate-independent single crystal plasticity theory developed by Anand and Kothari [8]. A

multiplicative decomposition of the deformation gradient tensor $\mathbf{F}$ into its elastic and plastic components, i.e., $\mathbf{F}^{\mathrm{e}}$ and $\mathbf{F}^{\mathrm{p}}$, is considered here as follows:

$$\mathbf{F} = \mathbf{F}^{\mathrm{e}}\mathbf{F}^{\mathrm{p}} \tag{1}$$

Two independent deformation mechanisms of elastic distortion of the crystal lattice and plastic slip accommodate the applied deformation. The macroscopic velocity gradient tensor $\mathbf{L}$ can be additively decomposed into the elastic and plastic components, i.e., $\mathbf{L}^{e}$ and $\mathbf{L}^{\mathrm{p}}$, respectively, as follows:

$$\mathbf{L} = \mathbf{L}^{e} + \mathbf{L}^{p} \tag{2}$$

The key idea of crystal plasticity is to link the plastic part of the velocity gradient to the superposition of shear deformation induced by crystallographic slip on multiple slip as follows:

$$\mathbf{L}^{\mathrm{p}} = \sum_{\alpha} \dot{\gamma}^{\alpha}\mathbf{S}^{\alpha}\,\mathrm{sign}(\tau^{\alpha}) \tag{3}$$

where $\dot{\gamma}^{\alpha}$ is the shearing rate on slip system α, τ^{α} is the resolved shear stress acting on the slip system α, and $\mathbf{S}^{\alpha}$ is the Schmid tensor for the slip system α, which can be defined as follows:

$$\mathbf{S}^{\alpha} = \mathbf{m}^{\alpha}\otimes\mathbf{n}^{\alpha} \tag{4}$$

where unit vectors $\mathbf{m}^{\alpha}$ and $\mathbf{n}^{\alpha}$ denote the slip direction and slip plane normal, respectively, in the deformed configuration.

The resolved shear stress on the slip system α can be obtained as follows:

$$\tau^{\alpha} = \boldsymbol{\sigma}\colon\mathbf{S}^{\alpha} \tag{4}$$

where $\boldsymbol{\sigma}$ is the Cauchy stress tensor.

The rate-independent yield surface of slip system α can be defined as follows:

$$f^{\alpha} = |\tau^{\alpha}| - s^{\alpha} \tag{5}$$

where s^{α} is the slip resistance on slip system α. Finally, the slip resistance evolution for slip system α can be obtained as follows:

$$\dot{s}^{\alpha} = \sum_{\beta} h^{\alpha\beta}\dot{\gamma}^{\beta} \tag{6}$$

where $h^{\alpha\beta}$ describes the variation of slip resistance for slip system α due to the slip rate on slip system β. The hardening moduli $h^{\alpha\beta}$ can be described as a power-law relationship considering the combined effect of work hardening and recovery as follows:

$$h^{\alpha\beta} = h_0^{\beta} q\left[1 - \frac{s^{\beta}}{s_s^{\beta}}\right]^{a^{\beta}} \tag{7}$$

where q is the latent hardening ratio ($q = 1$ in the case of $\alpha = \beta$), h_0^{β} denotes the hardening parameter for slip system β, s_s^{β} is the slip resistance at hardening saturation for slip system β, and a^{β} is a material constant for slip system β which governs the sensitivity of the hardening moduli to the slip resistance.

For this investigation, using the *PRISMS-Plasticity* code, a polycrystalline model of the Mg-2.4Nd alloy was generated as a stacked aggregate of single crystal eight-node cubic elements in a 6 x 7 x 9 = 378 finite element mesh. Each element is assigned a separate lattice orientation from the 376 far-field HEDM (ff-HEDM) identified initial grain orientations, with two orientations duplicated and element spatial arrangement randomly seeded. For the initial calibration simulation, the orientation distribution function of the sample is captured but local neighborhood crystallographic orientations and grain morphology are not. Future work will include use of the local neighborhood and grain morphologies.

Tensile loading and unloading displacements were applied at a fixed strain rate of $1\text{x}10^{-4}$ s^{-1}, and the degree of load drop at each measurement point set by global strain measurements from surface digital

image correlation (DIC). Deformation in the HCP crystal structure was modelled with four slip mechanisms including Basal $\langle a \rangle (\{0001\}\langle 11\bar{2}0 \rangle)$, Prismatic $\langle a \rangle (\{10\bar{1}0\}\langle 11\bar{2}0 \rangle)$, Pyramidal $\langle a \rangle (\{10\bar{1}1\}\langle 11\bar{2}0 \rangle)$, and Pyramidal $\langle c + a \rangle (\{11\bar{2}2\}\langle 11\bar{2}3 \rangle)$, with a latent hardening parameter of q = 1. The extruded basal texture of the Mg-2.4Nd alloy in this study results in basal poles aligned perpendicular to the extrusion direction, favourably orienting grains for twinning upon uniaxial compressive loading [9-13]. Deformation twinning at low tensile strains is not expected and were not included in this initial simulation. *PRISMS-Plasticity* has the capability for modelling twinning deformation [7]. The single crystal elastic constants used in the simulations are listed in Table 1. This *PRISMS-Plasticity* CPFE simulation was performed using 32 processors on the PRISMS FLUX cluster at the University of Michigan with a simulation time (wall time) of 2700 seconds. *PRISMS-Plasticity* has the capability of automatically uploading simulation results and analysis meta-data to the Materials Commons and this was accomplished.

Table 1. Mg elastic constants used in this study (GPa) [14]

C11	C12	C13	C33	C44
59.40	25.61	21.44	61.60	16.40

4. Results

Grain-level elastic strain tensors were tracked through the stacked volume through far-field spot diffraction analysis. Grain average stress tensors were calculated with the elastic stiffness constants listed in Table 1 and grain average orientation from ff-HEDM. The resolved shear stresses of Basal ⟨a⟩, Prismatic ⟨a⟩, Pyramidal ⟨a⟩, and Pyramidal ⟨a+c⟩ slip modes were calculated in each grain using its average stress. Next, in each grain and for each slip mode, the maximum resolved shear stress is determined. The values obtained are averaged for all grains and reported in Table 2 for each slip mode along with the corresponding standard deviation. The measured values given in Table 2 are at the 15% load drop point; the strains (load steps) listed are the initial strains prior to the 15% load drop. The average values of resolved shear stresses for all slip modes increase as the strain increases from 0.2 % to 0.5 % due to work hardening. This increase is also observed using the CPFE simulation as shown in Figure 2.

Since the basal slip mode is the dominant slip mechanism for the range of strains investigated, the data obtained for the basal mode is investigated further. Accordingly, the distribution of the resolved shear stresses corresponding to the basal mode for all grains is obtained using both HEDM and CPFE (at the 15% load drop point) at the strain load steps of 0.2% and 0.5%, as shown in Figure 2. At the 0.2% load step, the distribution of the resolved shear stresses ranges from 0 MPa to 30 MPa. At the 0.5% load step, the distribution of the resolved shear stresses spans from 0 MPa to 45 MPa. The wide range of basal resolved shear stresses observed for both strain values can be attributed the wide grain size distribution, magnesium extrusion texture, and the hcp crystal structure's extensive plastic anisotropy [15]. Similar spread in basal resolved shear stress distribution has been observed in other hcp materials such as Ti-7Al [3, 5].

In the case of the CPFE simulation, all grains are modelled to have a similar size. Accordingly, the distribution of basal resolved shear stress is sharp. Future plans for addition of grain size, grain morphology, and spatial distribution from nf-HEDM will integrate local grain neighborhood characteristics, more accurately accounting for local strain accommodation.

Figure 3 (a) presents the response of the sample during uniaxial tensile loading. It includes the stresses obtained from the DIC measurement, i.e., load divided by the cross-section area, the CPFE

simulation results, and the stress obtained from the HEDM results (after the 15% load drop). In the case of HEDM, one can obtain the average stress of each grain using its average strain. Here, due to the lack of experimental data regarding to the size of each grain corresponding to each strain, it is assumed that all grains have equal size. Accordingly, the sample stress can be obtained by averaging the stresses for all grains. The stresses obtained from HEDM for 0.2 % and 0.5% (initial) strains are 20% and 13% lower than those of the DIC experiment, respectively. The observed differences can be attributed to the grain size distribution and elastic moduli used in the calculations. First, it is assumed here that the grains have a similar size, which is not precise. Second, the elastic modulus incorporated here is for pure Mg, which is slightly different from the Mg-2.4Nd alloy. The difference is not considered to be related to the accuracy of the experimental framework. Future work will integrate weighting of grain size from near field HEDM and simulated Mg-2.4Nd moduli [3-5].

Fig. 3. (a) shows that the stress-strain response of the sample can be successfully captured using CPFE. Furthermore, the relative slip activity of the sample obtained by CPFE simulation is presented in Figure. 3 (b). As expected, the basal mode is dominant at low strains with minor activation of prismatic slip and pyramidal accommodation of c-axis deformation [15-23].

Table 2. Average ff-HEDM resolved shear stress for 0.2% and 0.5% strain load steps, solution heat treated Mg-2.4Nd

	Average Resolved Shear Stress (MPa)			
Load Step	Basal	Prismatic	Pyramidal <a>	Pyramidal <c+a>
0.2% Strain	10.7 ± 4.7	9.1 ± 5.6	12.0 ± 5.0	14.6 ± 6.9
0.5% Strain	17.4 ± 10.3	19.6 ± 12.9	23.7 ± 12.3	26.1 ± 11.7

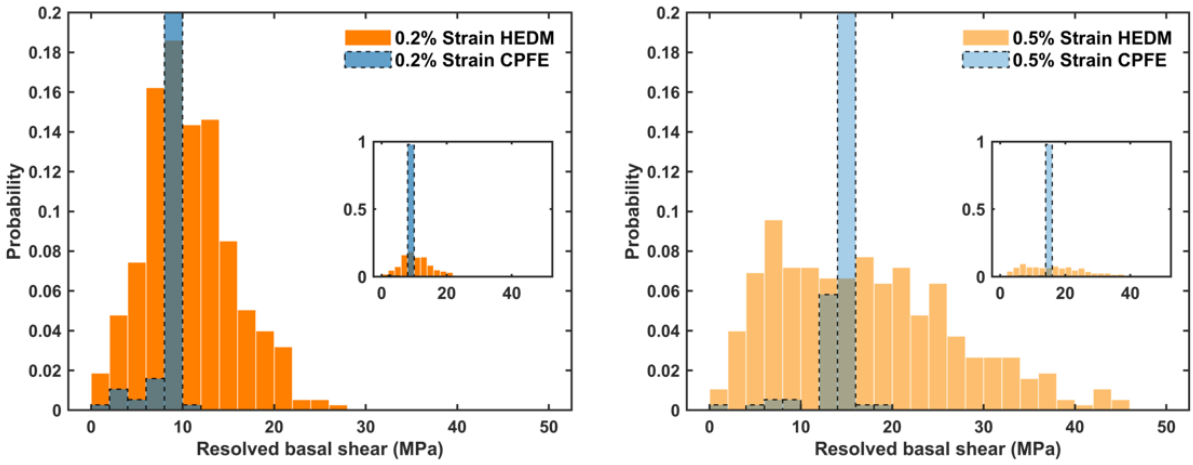

Figure 2. Distribution of the resolved shear stress for the basal slip mode in every grain tracked in solution heat treated Mg-2.4Nd. CPFE simulated distribution overlaid in dark blue (0.2% strain - left) and light blue (0.5% strain - right). (For interpretation of color, the reader is directed to the web version of the article). Note: HEDM and CPFE results are at 15% load drop condition for each strain step.

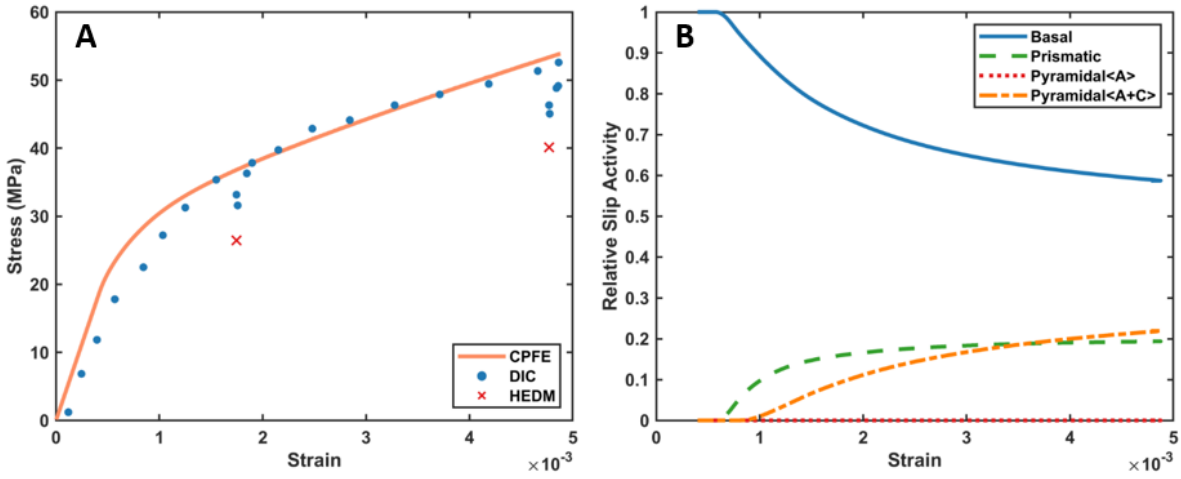

Figure 3. Uniaxial response of the solution heat treated Mg-2.4Nd sample during uniaxial tensile loading: (a) The stress-strain response is obtained using DIC, CPFE simulation, and (after the 15% load drop) the far-field HEDM; (b) Relative slip activity obtained by CPFE.

5. Publishing 4D Information Using the Materials Commons

The Materials Commons is an information repository and virtual collaboration space for curating, archiving and disseminating information from experiments and computations [24]. It is an integral part of the PRISMS framework [1] and is readily available to the global materials community at https://materialscommon.org. It provides solutions to the data problems facing the 4D materials researcher. Synchrotron-based 4D HEDM experiments require proposals, scheduling, sample preparation and complex data analysis making these datasets relatively difficult and costly to secure. The data contained in these datasets is also rich, requires large storage and is often incompletely analysed – thus reuse of these datasets is important for continuously improving our understanding of the phenomena uncovered by these important measurements. Similarly, when these experiments are analysed using advanced computational methods it is instructive to understand all of the modelling parameters used in these simulations. The Materials Commons is aimed at assisting the 4D community in secure storage and re-use of these valuable datasets.

The Materials Commons is designed to capture meta-data seamlessly either during an experiment or after an experiment or simulation is completed. It has a straight forward web-based user-interface that guides the user through data and meta-data upload. Data can be automatically uploaded from spreadsheets or by using the Materials Commons web user interface or using the Materials Commons Application Program Interface (API). The results of *PRISMS-Plasticity* simulations can be automatically stored in the Materials Commons in a consistent format using the Materials Commons API. For large datasets typical of HEDM information, the Materials Commons uses the Globus file transfer service for fast, secure data transfers [25]. Custom templates have been designed for use with HEDM from CHESS and APS beamlines. These templates are readily adaptable and customizable for other synchrotron facilities. When ready for publication, datasets can be easily formed and published with the push of a virtual button. With over 400Tb of storage, the Materials Commons is capable of storing and publishing large datasets. Future embodiments of the Materials Commons will provide access to large datasets stored on “cloud services”.

6. Summary

The evolution of deformation in a Mg-Nd alloy has been investigated using 4D HEDM at CHESS and full field crystal plasticity simulation using the *PRISMS-Plasticity* CPFE Code. The base microstructural RVE for the CPFE simulation was a simple grid microstructure which captures the overall texture of the experimental sample but not the local grain neighborhoods and grain morphologies. The average stress-strain response is well predicted by the CPFE simulation. At global strains up to 0.5%, deformation is dominated by basal slip. In addition to the average stress-strain response, resolved basal stress distributions have been characterized experimentally and CPFE for each grain in the solution treated sample. The CPFE simulated stress distribution is substantially narrower than that experimentally determined by HEDM. This indicates the need for more precise RVE in the CPFE to include local grain neighborhoods and morphologies and intergranular misorientation developments [26]. The results of these HEDM experiments and *PRISMS-Plasticity* simulations can be readily stored in the Materials Commons and provided to the wider materials community. Both the *PRISMS-Plasticity* code and the Materials Commons are available as open-source software and key components of the PRISMS framework for use in accelerating the prediction of material responses.

Acknowledgements
This work was supported by the U.S. Department of Energy, Office of Basic Energy Sciences, Division of Materals Sciences and Engineering under Award #DE-SC0008637 as part of the Center for PRedictive Integrated Structural Materials Science (PRISMS Center) at University of Michigan. This work is based upon research conducted at the Cornell High Energy Synchrotron Source (CHESS) which is supported by the National Science Foundation under award DMR-1332208. We acknowledge with appreciation CANMETMaterials who provided the materials used in this study.

References

[1] Aagesen L K, Adams J F, Allison J E, Andrews W B, Araullo-Peters V, Berman T, Chen Z, Daly S, Das S, DeWitt S, et al 2018 JOM 70 2298–314
[2] Shade P A, Blank B, Schuren J C, Turner T J, Kenesei P, Goetze K, Suter R M, Bernier J V, Fai Li S, Lind J, et al 2015 Rev. Sci. Instrum. 86 93902-1-93902-8.
[3] Pagan D C, Shade P A, Barton N R, Park J S, Kenesei P, Menasche D B and Bernier J V. 2017 Acta Mater. 128 406–17.
[4] Guillen D P, Pagan D C, Getto E M and Wharry J P 2018 *Mater. Sci. Eng. A* **738** 380–8.
[5] Pagan D C, Bernier J V, Dale D, Ko J Y P, Turner T J, Blank B and Shade P A 2018 *Scr. Mater.* **142** 96–100.
[6] Bernier J V, Barton N R, Lienert L J and Miller M P, 2011 *Journal of Strain Analysis* **46** 527-47.
[7] Yaghoobi M, Ganesan S, Sundar S, Lakshmanan A, Rudraraju S, Allison J and Sundararaghavan V 2019, in press, *Computational Materials Science, https://doi.org/10.1016/j.commatsci.2019.109078.*
[8] Anand L and Kothari M 1996 *J. Mech. Phys. Solids* **44** 525-58.
[9] Wu L, Jain A, Brown D W, Stoica G M, Agnew S R, Clausen B, Fielden D E and Liaw P K 2008 *Acta Mater.* **56** 688–95.
[10] Murphy-Leonard A D, Pagan D C, Beaudoin A, Miller M P and Allison J E 2019 *Int. J. Fatigue* **125** 314–23.
[11] Mirza F A, Chen D L, Li D J and Zeng X Q 2013 *Mater. Sci. Eng. A* **575** 65–73.
[12] Brown D W, Jain A, Agnew S R and Clausen B 2007 *Mater. Sci. Forum* **539–543** 3407–13.
[13] Kumar AM, Beyerlein I J and Tome C N 2017 J. Alloys Compd. 695 1488–97.
[14] Zhang J and Joshi S P 2012 *J. Mech. Phys. Solids* **60** 945–72.
[15] Agnew S R and Duygulu Ö 2005 *Int. J. Plast.* **21** 1161–93.

[16] Wang H, Boehlert C J, Wang Q D, Yin D D and Ding W J 2016 *Mater. Charact.* **116** 8–17.
[17] Agnew S R, Tomé C N, Brown D W, Holden T M and Vogel S C 2003 *Scr. Mater.* **48** 1003–8
[18] Koike J, Kobayashi T, Mukai T, Watanabe H, Suzuki M, Maruyama K and Higashi K 2003 *Acta Mater.* **51** 2055–65.
[19] Jain A and Agnew S R 2007 *Mater. Sci. Eng. A* **462** 29–36.
[20] Beyerlein I J, Capolungo L, Marshall P E, McCabe R J and Tome C N 2010 *Philos. Mag.* **90** 2161–90.
[21] Cheng J and Ghosh S 2015 *Int. J. Plast.* **67** 148–70.
[22] Cheng J, Shen J, Mishra R K and Ghosh S 2018 *Acta Mater.* **149** 142–53.
[23] Kadiri H El, Kapil J, Oppedal A L, Hector L G, Agnew S R, Cherkaoui M and Vogel S 2013 *Acta Mater.* **61** 3549–63.
[24] Puchala B, Tarcea G, Marquis E A, Hedstrom M, Jagadish H V, Allison, J E 2016 *JOM* **68** 2035-44.
[25] Kettimuthu R, Liu Z, Wheeler D, Foster I, Heitmann K and Cappello F 2018 Future Generation Computer Systems 88 191–8.
[26] Acar P, Ramazani A and Sundararaghavan V 2017 *Metals* **7(11)** 459.